On structural phase transitions in *n*-butylammonium chloroantimonate(III) and chlorobismuthate(III) crystals: x-ray, differential scanning calorimetry, dilatometric and dielectric dispersion studies

1997 J. Phys.: Condens. Matter 9 627

(http://iopscience.iop.org/0953-8984/9/3/004)

J. Phys.: Condens. Matter **9** (1997) 627–645. Printed in the UK PII: S0953-8984(97)74919-1

On structural phase transitions in *n*-butylammonium chloroantimonate(III) and chlorobismuthate(III) crystals: x-ray, differential scanning calorimetry, dilatometric and dielectric dispersion studies

P Ciąpała†, R Jakubas†, G Bator†, J Zaleski‡, A Pietraszko§, M Drozd§ and J Baran§

† Faculty of Chemistry, University of Wrocław, 50-383 Wrocław, Joliot Curie 14, Poland
‡ Institute of Chemistry, University of Opole, 45-951 Opole, Oleska 48, Poland
§ Institute of Low Temperature and Structure Research, Polish Academy of Science, Okólna 2, 50-422 Wrocław, Poland

Received 29 May 1996, in final form 28 August 1996

Abstract. Numerous structural phase transitions are detected in new crystals of the *n*-butylammonium compounds: $(n\text{-}C_4H_9NH_3)_2SbCl_5$, $(n\text{-}C_4H_9NH_3)_2BiCl_5$ and $(n\text{-}C_4H_9NH_3)_3SbCl_6$ by means of differential scanning calorimetry, dilatometric and dielectric dispersion (1 kHz–1 MHz) studies. For the transitions the basic thermodynamic data are determined. Interesting dielectric properties are found in a metastable (β) form of the $(n\text{-}C_4H_9NH_3)_2BiCl_5$ crystals. Debye-like dispersion of the electric permittivity between 30 and 800 MHz is observed around the 310 K phase transition for this crystal. The activation energy of the reorientation of the *n*-butylammonium cations is found to be 16 kJ mol^{-1}. The structure of $(n\text{-}C_4H_9NH_3)_2BiCl_5$ (α form) has been refined to $R = 0.0439$ and shows isolated $Bi_2Cl_{10}^{4-}$ units and two non-equivalent *n*-butylammonium units. One of these cation possesses dynamical disorder. Most of the phase transitions in the title crystals are classified as an 'order–disorder' type and connected with a reorientational motion of the *n*-butylammonium cations.

1. Introduction

Alkylammonium halogenoantimonates(III) and halogenobismuthates(III) of the general formula $R_xM_yX_z$ (R = alkylammonium; M = Sb or Bi; X = Cl, Br or I) have been extensively investigated [1–3]. Some of the crystals, belonging to the $R_3M_2X_9$ subgroup containing organic cations which are small in size, revealed ferroelectric properties [4–6]. The other subgroup $(CH_3NH_3)_5Bi_2X_{11}$ (X = Cl or Br) also revealed interesting properties (ferroelectric and non-linear optical), rendering them promising materials from the viewpoint of applications [7, 8]. The ferroelectric activity in these organic–inorganic crystals is related to ordering processes of alkylammonium cations. The crystals with bulky cations were only fragmentarily studied. Recently, interesting sequences of phase transitions have been discovered for a new group of crystals of the isopropylammonium compounds of chemical formula $(i\text{-}C_3H_7NH_3)_2MX_5$ (X = Cl or Br; M = Sb or Bi). They were attributed to the ordering of the isopropylammonium cations [9]. The cations were found to perform a flipping motion between two positions. Two salts containing *n*-propylammonium cations, namely $(n\text{-}CH_3H_7NH_3)_2SbBr_5$ [10, 11] and $(n\text{-}C_3H_7NH_3)_2BiBr_5$ [12], revealed a

0953-8984/97/030627+19$19.50

very complex sequence of phase transitions (five and three phase transitions, respectively) accompanied by a change in the cation dynamics as well. Very recently, the dynamical properties near the structural phase transition at 232 K have been described for the next new n-propylammonium derivative, $(n\text{-}C_3H_7NH_3)_3Sb_2Cl_9$ [13]. Dielectric dispersion studies in the microwave frequency region of this crystal revealed a single relaxator associated with the flipping motion of the alkyl chains around their long axis.

This paper reports the results of the structural, differential scanning calorimetry (DSC), dilatometric and dielectric measurements on crystals of butylammonium compounds: $(n\text{-}C_4H_9NH_3)_2SbCl_5$, $(n\text{-}CH_4H_9NH_3)_2BiCl_5$ and $(n\text{-}CH_4H_9NH_3)_3SbCl_6$, in order to complete a systematic experimental study of the structural phase transition sequence in a new halogenoantimonate and halegenobismuthate family containing bulky alkylammonium cations. With these studies we want to establish the influence of the alkylammonium chain of organic cations on the dynamical and particularly on the polar properties of the crystals.

2. Experimental details

All crystals of the *n*-butylammonium compounds were obtained from the aqueous solutions containing stoichiometric ratios of *n*-butylamine and $SbCl_3$ or $BiCl_3$ and a large excess of HCl. Single crystals of $(n\text{-}C_4H_9NH_3)_2BiCl_5$ were obtained by slow evaporation of the aqueous solutions at room temperature.

DSC measurements were carried out using a Perkin–Elmer DSC-7 differential scanning calorimeter with a heating and cooling rate of 10 K min^{-1}.

Linear thermal expansion was measured using a Perkin–Elmer TMS-2 thermomechanical analyser. The samples used in the measurements were prepared in the form of thin plates (5 mm × 5 mm × 1.5 mm). The anomalies in the vicinity of the phase transitions were always reproducible to within 10% for each sample. The accuracy of thermal expansion determination was about 3%.

For dielectric measurements, polycrystalline samples of $(n\text{-}CH_4H_9NH_3)_2SbCl_5$ and $(n\text{-}C_4H_9NH_3)_3SbCl_6$ were used and, for $(n\text{-}C_4H_9NH_3)_2BiCl_5$, single-crystal samples of dimensions 8 mm × 2 mm × 0.5 mm were cut perpendicular to the *c* axis. The plates were silver painted. Complex electric permittivity was measured with an HP 4284A precision *LCR* meter in the frequency range 500 Hz–1 MHz and a HP 4191A impedance analyser in the frequency range 30–800 MHz. The measurements were performed in the temperature range 100–370 K. The temperature of the specimen was varied continuously at a rate of 0.1 K min^{-1} in the vicinity of T_c and 0.5 K min^{-1} elsewhere in the low-frequency region. In the high-frequency region the temperature was stabilized and controlled with a UNIPAN temperature controller type 650 with fluctuation less than ±0.1 K. The overall errors for the real part of the complex electric permittivity were less than 5% and 10% in the low- and high-frequency regions, respectively.

Data structure determination was collected on a KM-4 KUMA diffractometer with Mo Kα radiation ($\lambda = 0.710\,73$ Å; graphite mononochromator). Lattice parameters were refined from setting angles of 24 reflections in the $18^\circ < 2\theta < 29^\circ$ range. A summary of the measurement parameters is presented in table 1. A total of 7098 reflections with $4^\circ < 2q < 50^\circ$ were collected using the ω–q scan technique (scan speed, 0.025–0.1° s^{-1}; scan width, 1.4–1.56°) of which 1431 had $F_o > 4\sigma(/F_o/)$ and were used for structure determination. Two control reflections measured after an interval of 50 reflections show that the intensity variation was negligible. Lorentz, polarization and semiempirical absorption corrections were applied. The SHELXTL PC program [14] was used for all the structure calculations and drawings.

Table 1. Crystal data for the α form of $(n\text{-}C_4H_9NH_3)_2BiCl_5$ and the summary of the measurement parameters.

Empirical formula	$(n\text{-}C_4H_9NH_3)_2BiCl_5$
Temperature (K)	298
Crystal size (mm × mm × mm)	0.3 × 0.4 × 0.4
Crystal system	Monoclinic
Space group	$P2_1/c$
Unit-cell dimensions	
a (Å)	11.983(3)
b (Å)	12.660(4)
c (Å)	12.718(2)
β (deg)	98.40(3)
Volume (Å^3)	1909(1)
Z	4
Formula weight	534.5
Density (calculated) (g cm^{-3})	1.860
Density (measured) (g cm^{-3})	1.85(1)
Absorption coefficient (mm^{-1})	9.90
Semiempirical absorption correction	
Minimum transmission	0.06
Maximum transmission	0.18
Index ranges	$-15 < h < 0$
	$-15 < k < 15$
	$-14 < l < 14$
Number of reflections collected	7098
Number of independent reflections	2838($R_{int} = 4.28\%$)
Number of observed reflections	1431($F > 4.0\sigma(F)$)
Refinement method	Full-matrix least-squares
Quantity minimized	$\Sigma_w(F_o - F_c)^2$
Weighting scheme	$w^{-1} = \sigma^2(F)$
Number of parameters refined	158
Final R indices (observed data)[a]	$R = 4.39\%$, $R_w = 4.55\%$
Goodness of fit	1.77
Data-to-parameter ratio	8.3:1
Largest-difference peak (electrons Å^{-3})	0.83
Largest-difference hole (electrons Å^{-3})	−0.65

[a]
$$R = \frac{\sum |F_o - F_c|}{\sum F_o} \qquad R_w = \frac{\sum |F_o - F_c\sqrt{\text{weight}}|}{\sum F_o\sqrt{\text{weight}}}.$$

3. Results

3.1. X-ray data

The centrosymmetrical $P2_1/c$ space group follows from systematic absences of reflections. The structure was solved by the Patterson method and subsequent difference Fourier synthesis. It was refined by the full-matrix least-squares method using anisotropic temperature factors. Hydrogen atoms connected to N atoms were placed from geometric considerations and were not refined. The n-butyllammonium cations are characterized by large thermal motions which are reflected in their large temperature factors. The positional parameters of refined atoms are presented in table 2.

The anionic sublattice of $(n\text{-}C_4H_9NH_3)_2BiCl_5$ is composed of isolated $Bi_2Cl_{10}^{4-}$ units composed of two $BiCl_6^{3-}$ octahedra sharing an edge as presented in figure 1(a). There are

Table 2. Atomic coordinates and equivalent isotropic displacement coefficients of refined atoms of $(n\text{-}C_4H_9NH_3)_2BiCl_5$ at 298 K (the hydrogen atoms of NH_3^+ groups were placed from geometric considerations). The equivalent isotropic U is defined as one third of the trace of the orthogonalized U_{ij} tensor.

Atom	x ($\times10^{-4}$)	y ($\times10^{-4}$)	z ($\times10^{-4}$)	U_{eq} ($\times10^{-3}$ Å^2)
Bi(1)	1069(1)	156(1)	1600(1)	65(1)
Cl(1)	731(6)	626(4)	3645(4)	92(2)
Cl(2)	665(6)	−1833(4)	2039(4)	85(2)
Cl(3)	1351(6)	2262(4)	1102(4)	83(2)
Cl(4)	1241(6)	−444(4)	−650(4)	82(2)
Cl(5)	3016(6)	−91(6)	2216(6)	117(2)
N(1)	1037(15)	6793(12)	−190(14)	87(3)
C(1)	2221(25)	6754(22)	116(22)	143(3)
C(2)	2446(3)	5097(27)	1015(29)	229(3)
C(31)	3135(42)	5028(42)	1745(40)	209(3)
C(32)	3673(43)	6148(43)	1761(41)	219(3)
C(4)	3823(31)	4913(32)	970(29)	287(3)
N(2)	1992(18)	3015(15)	3588(14)	101(3)
C(5)	3094(25)	2899(27)	3634(24)	161(3)
C(6)	3688(31)	3243(34)	4584(30)	260(3)
C(7)	4780(29)	3031(32)	4611(28)	235(3)
C(8)	5399(32)	3379(31)	5772(28)	298(3)
H(1A)	803	7266	−730	100
H(1B)	833	6140	−428	100
H(1C)	760	6945	441	100
H(2A)	1662	2768	2924	100
H(2B)	1736	2685	4156	100
H(2C)	1876	3714	3630	100

two crystallographically non-equivalent *n*-butylammonium cations (see figures 1(b) and (c)). They are connected to the anionic sublattice by N–H . . . Cl hydrogen bonds. It should be noted that the cations are located in such a way that the alkyl chains are directed towards each other, while N atoms face towards the anionic units. The projection of the crystal structure of $(n\text{-}C_4H_9NH_3)_2BiCl_5$ on the **a**–**b** plane is presented in figure 2.

One of the cations (N(2)) is ordered and the other (N(1)) disordered. The disorder is realized by splitting of the C(3) carbon atom between two sites (see figure 1(b)). They were refined with half-occupancy. The conformation of the ordered N(2) cation is typical of *n*-alkane chains. Successive nitrogen and carbon atoms are in *trans* conformation to each other. Dihedral angles N(2)–C(5)–C(6)–C(7) = 176(3)° and C(5)–C(6)–C(7)–C(8) = −176(3)° are close to the theoretical ±180°. The disordered N(1) cation has a *trans* conformation on the C(2) atom, while on the C(3) atom it has a *gauche* conformation. Dihedral angles N(1)–C(1)–C(2)–C(31) = 156(8)° and N(1)–C(1)–C(2)–C(32) = −157(3)°. This may suggest that the ethyl group of the alkylammonium chain of this cation undergoes reorientation around the C(2)–C(1) bond.

The bond lengths and angles of the $(n\text{-}C_4H_9NH_3)_2BiCl_5$ anion are presented in table 3. The bismuth atoms are at the centres of distorted octahedra with Bi–Cl bonds in the 2.50–3.01 Å range. The longest Bi–Cl contacts (2.843(6) and 3.014(7) Å) correspond to bonds involving bridging chlorine atoms, and the shortest (2.620(6) and 2.500(7) Å) to bonds involving terminal chlorine atoms opposite to the bridging chlorine atoms. The bond angles

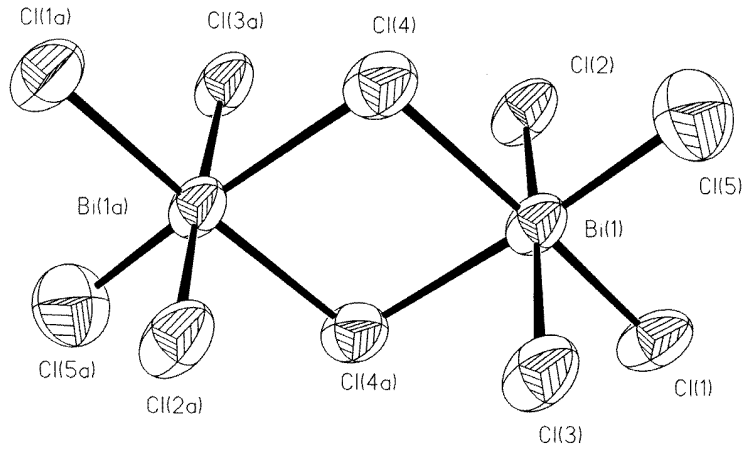

(a)

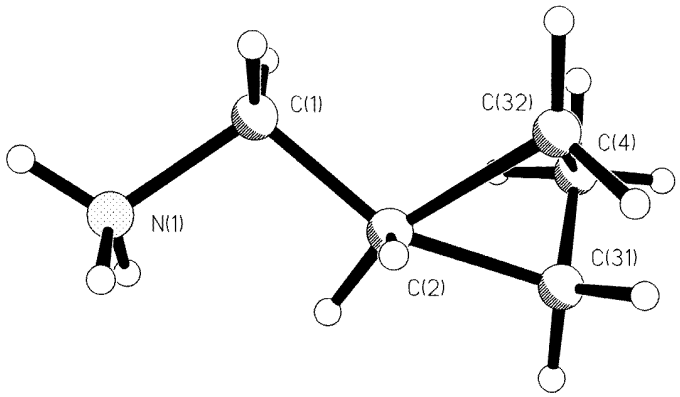

(b)

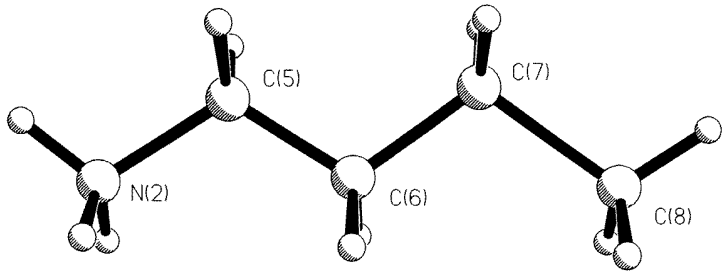

(c)

Figure 1. (a) Structure of the $Bi_4Cl_{10}^{4-}$ anion; (b), (c) two crystallographically non-equivalent *n*-butylammonium cations with the atomic numbering scheme.

of the anion are in the range 83.2–96.8°. They vary from the undistorted value of 90° for the ideal octahedron.

The lengths and angles of the cations are not included in table 3 since they are not precisely determined, because of their large thermal motions.

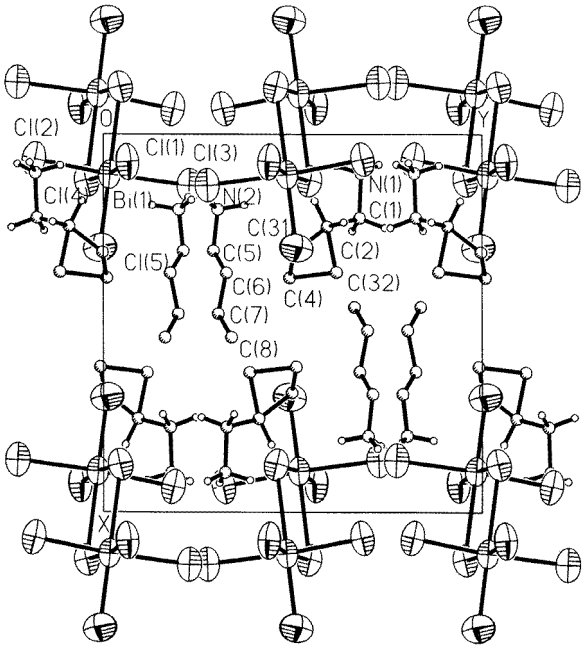

Figure 2. Projection of the crystal structure of the α form of $(n\text{-}C_4H_9NH_3)_2BiCl_5$ on the **a**–**b** plane.

Table 3. Bond distances and angles of the α form of $(n\text{-}C_4H_9NH_3)_2BiCl_5$ at 298 K.

Atoms[a]	Bond distance (Å)	Atoms[a]	Bond angle (deg)
Bi(1)–Cl(1)	2.617(6)	Cl(1)–Bi(1)–Cl(2)	88.1(2)
Bi(1)–Cl(2)	2.639(5)	Cl(1)–Bi(1)–Cl(3)	91.6(2)
Bi(1)–Cl(3)	2.767(6)	Cl(1)–Bi(1)–Cl(4)	174.6(2)
Bi(1)–Cl(4)	2.841(6)	Cl(1)–Bi(1)–Cl(4′)	92.4(2)
Bi(1)–Cl(4')	3.012(7)	Cl(1)–Bi(1)–Cl(5)	92.5(2)
Bi(1)–Cl(5)	2.498(7)	Cl(2)–Bi(1)–Cl(3)	176.3(2)
		Cl(2)–Bi(1)–Cl(4′)	89.1(2)
		Cl(2)–Bi(1)–Cl(4)	88.8(2)
		Cl(2)–Bi(1)–Cl(5)	92.0(2)
		Cl(3)–Bi(1)–Cl(4)	91.3(2)
		Cl(3)–Bi(1)–Cl(4′)	87.3(2)
		Cl(3)–Bi(1)–Cl(5)	91.7(2)
		Cl(4)–Bi(1)–Cl(4′)	83.1(2)
		Cl(4)–Bi(1)–Cl(5)	92.0(2)
		Cl(5)–Bi(1)–Cl(4′)	175.1(2)
		Bi(1)–Cl(4)–Bi(1′)	96.9(2)

[a] Symmetry code: $'$, $-X$, $-Y$, $-Z$.

Bismuth(III) and antimony(III) atoms possess a lone electron pair. It is not stereochemically active occupying an orbital of a spherical symmetry type s. The lone electron pair may easily be deformed from the initial symmetry as a result of the formation of M–X–M (M = Bi, or Sb; X = Cl, Br or I) bonds, by the packing interaction and, as

recently shown, also by the formation of hydrogen bonds [15]. This results in variation in the Bi–Cl bond lengths.

The lone electron pair of trivalent bismuth results in lengths of Bi(III)–X bonds which appear to be considerably longer than those for the pentavalent bismuth atom. For instance in the case of ideal octahedral coordination all Bi(III)–Cl bond lengths are equal to 2.686(8) Å, while for bonds involving Bi(V)–Cl they are equal to 2.406(23) Å [16]. The formation of Bi(III)–Cl–Bi(III) bonds distorts the ideal octahedron in such a way that bonds involving bridging chlorine atoms became longer (and weaker) in comparison with those involving terminal chlorine atoms. The displacement of the lone electron pair towards bridging chlorine atoms results in shortening of the Bi–Cl bonds located opposite. This phenomenon is known as a *trans* effect. Thus one should expect the Bi–Cl bond lengths in the $Bi_2Cl_{10}^{4-}$ unit to fall into three clearly defined ranges. Such a situation is found in a related compound $(C_2H_{10}N_2S)_2(Bi_2Cl_{10}).4H_2O$ [17]. The Bi(III)–Cl bridging bonds are the longest (2.844(5) and 2.866(4) Å); those located opposite are the shortest (2.606(4) and 2.597(5) Å) and the others are of medium lengths (2.715(4) and 2.709(4) Å) and close to the undistorted value for an ideal octahedron.

In our case the lengths of the bonds in the anionic unit are additionally distorted owing to formation of the N–H . . . Cl hydrogen bonds. The hydrogen bond geometry is presented in table 4.

Table 4. Hydrogen bond geometry in the α form of $(n\text{-}C_4H_9NH_3)_2BiCl_5$.

Atoms[a]	N–H (Å)	H . . . Cl (Å)	N . . . Cl (Å)	Angle (deg)
N(1)–H(1B) . . . Cl(1′)	0.90	2.49(1)	3.37(2)	163(2)
N(1)–H(1C) . . . Cl(2″)	0.90	2.48(1)	3.28(2)	149(2)
N(2)–H(2A) . . . Cl(3)	0.90	2.25(1)	3.12(2)	162(20)
N(2)–H(2B) . . . Cl(3‴)	0.90	2.45(2)	3.25(2)	149(2)
N(2)–H(2C) . . . Cl(4‴)	0.90	2.54(2)	3.39(2)	159(2)

[a] Symmetry codes: ′, X, $0.5 - Y$, $Z - 0.5$; ″, X, $1 + Y$, Z; ‴, X, $0.5 - Y$, $Z + 0.5$.

The three strongest N–H . . . Cl hydrogen bonds of $(n\text{-}C_4H_9NH_3)_2BiCl_5$ involve Cl(2) and Cl(3) atoms. Two of them, namely N(1′)–H(1C′) . . . Cl(2) and N(2′)–H(2B′) . . . Cl(3) are almost equally strong. Since they are located opposite the Bi(1) atom and are almost equally strong, therefore they do not distort the Bi(1)–Cl(2) and Bi(1)–Cl(3) bond lengths. the third, namely N(2)–H(2A) . . . Cl(3), being the strongest, shifts the lone pair on the Bi(1) atom towards the N(2) atom and as a result the Bi(1)–Cl(3) bond length increases by about 0.06 Å (from 2.71 to 2.767(6) Å). The opposite Bi(1)–Cl(2) bond due to the *trans* effect is shortened to 2.639(5) Å, also by roughly 0.06 Å in comparison with lengths characteristic of an almost undistorted bond in $(C_2H_{10}N_4S)_2(Bi_2Cl_{10}).4H_2O$. Two remaining hydrogen bonds (table 4) involve Cl(4) and Cl(1) which are located opposite Bi(1) (figure 3). They do not elongate the Bi(1)–Cl(4) and Bi(1)–Cl(1) lengths since they are located opposite each other and at almost 90° to the corresponding Bi–Cl bonds. As a result the Cl(4) atom is shifted slightly down and the Cl(1) atom slightly up (see figure 4). However, this leads to elongation of the Bi(1A)–Cl(4) bond from 2.86 to 3.012(7) Å and shortening of the bond located opposite from 2.60 to 2.498(7) Å in comparison with those in the $(C_2H_{10}N_4S)_2(Bi_2Cl_{10}).4H_2O$ crystal [17].

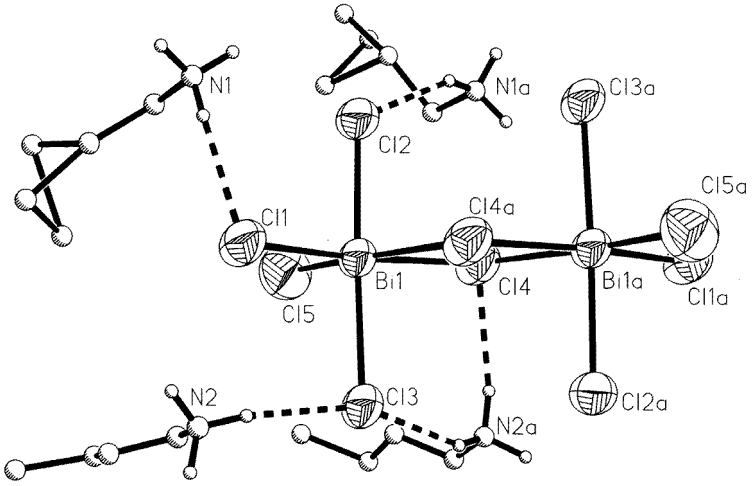

Figure 3. Scheme of the hydrogen bond system in the α form of $(n\text{-}C_4H_9NH_3)_2BiCl_5$.

The observed changes in B–Cl bond lengths caused by hydrogen bonds may be explained as a result either of deformation of spherical symmetry of the lone electron pair on Bi atoms or of a shift in the spherical pair related to the position of central Bi atom.

An attempt to solve the crystallographic structure of the metastable β form of the $(n\text{-}C_4H_9NH_3)_2BiCl_5$ crystal was unsuccessful because the phase transition at 370 K is always accompanied by a drastic breaking of the single crystal.

3.2. Differential scanning calorimetry measurements

The DSC curves for the $(n\text{-}C_4H_9NH_3)_3SbCl_6$ crystal recorded on heating and cooling runs are shown in figure 4(a). A distinct thermal anomaly at 322 K on heating (317 K on cooling), which is perfectly reproducible and reversible indicates a first-order phase transition. The transition enthalpy and entropy determined on heating from the peak area are given below in table 5.

The DSC plots on cooling and heating between 150 and 340 K for the $(n\text{-}C_4H_9NH_3)_2SbCl_5$ crystals are shown in figure 4(b). Two peak are observed at 229 and 315 K (temperatures on heating). The former peak is quite sharp, exhibiting a c_p 'tail' stretching back to 190 K, whereas the latter is broad with a peak temperature of about 315 K.

A very complex sequence of phase transitions was found for the $(n\text{-}C_4H_9NH_3)_2BiCl_5$ crystals. No heat anomaly is observed on the DSC curve measured for the fresh sample on cooling below room temperature down to 100 K. When the sample is heated above room temperature, one can observe a broad peak, the onset of which appears at about 350 K and the maximum at 370 K (the $\alpha \rightarrow \beta$ phase transition). This anomaly is irreversible and may be related to the structural phase transition exhibiting mixed features of the second- and first-order type. In the next cooling run at least four phase transitions in the β metastable form of the $(n\text{-}C_4H_9NH_3)_2BiCl_5$ crystal appear (see figure 5).

All the peaks on the DSC curves for $(n\text{-}C_4H_9NH_3)_2BiCl_5$ are well reproducible and reversible. We should notice a complex shape of the heat anomaly at 213 K (on cooling) which could suggest an overlapping of two peaks. However, there is only a single peak at 215 K during the heating scan. The present DSC experiment shows also that it is sufficient

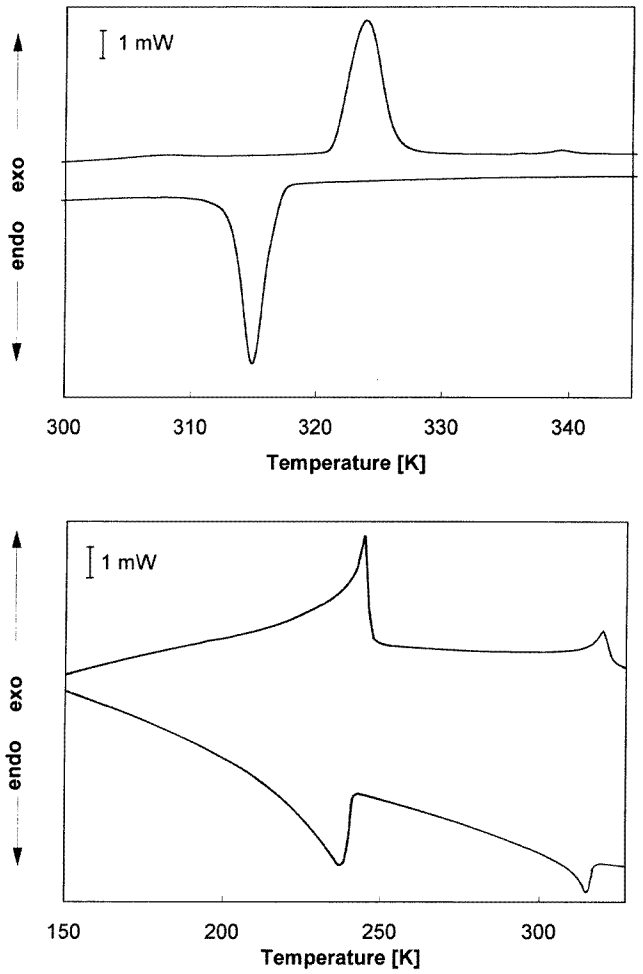

Figure 4. (a) DSC curves of the $(n\text{-}C_4H_9NH_3)_3SbCl_6$ crystal recorded on heating and cooling (sample mass, 5.6 mg; scanning rate, 10 K min^{-1}); (b) DSC curves of the $(n\text{-}C_4H_9NH_3)_2SbCl_5$ crystal recorded on heating and cooling (sample mass, 26.9 mg; scanning rate, 10 K min^{-1}).

to heat the fresh sample to a temperature corresponding to the onset (i.e. 350 K) of the anomaly to observe the phase transition sequence as presented in figure 5. However, only the anomalies at 310 and 215 K are well shaped whereas the reamaining anomalies are hardly visible. The 250 K phase transition was characterized by a relatively small value of $\Delta H = 0.05$ kJ mol^{-1}. In spite of its small amplitude, the temperature hysteresis of the phase transition is rather distinct ($\Delta T \approx 6$ K) which readily confirms the first-order type of the phase transition.

The thermal parameters of all studied crystals are summarized in table 5. The order of the phase transition was determined from the shape of the observed DSC anomaly and from the observed thermal hysteresis extrapolated linearly to zero scanning rate. Several phase transitions are accompanied by large entropy changes $-\Delta S \geqslant 5.7$ J mol^{-1} K^{-1} ($\Delta S = R \ln 2$), which suggests the order–disorder character of the phase transitions. The phase transitions characterized by a small ΔS-value ($\Delta S \leqslant 1$ J mol^{-1} K^{-1}, i.e. for $(n\text{-}C_4H_9NH_3)_2SbCl_5$ at 315 K and for $(n\text{-}C_4H_9NH_3)_2BiCl_5$ at 250 and 232 K) are considered

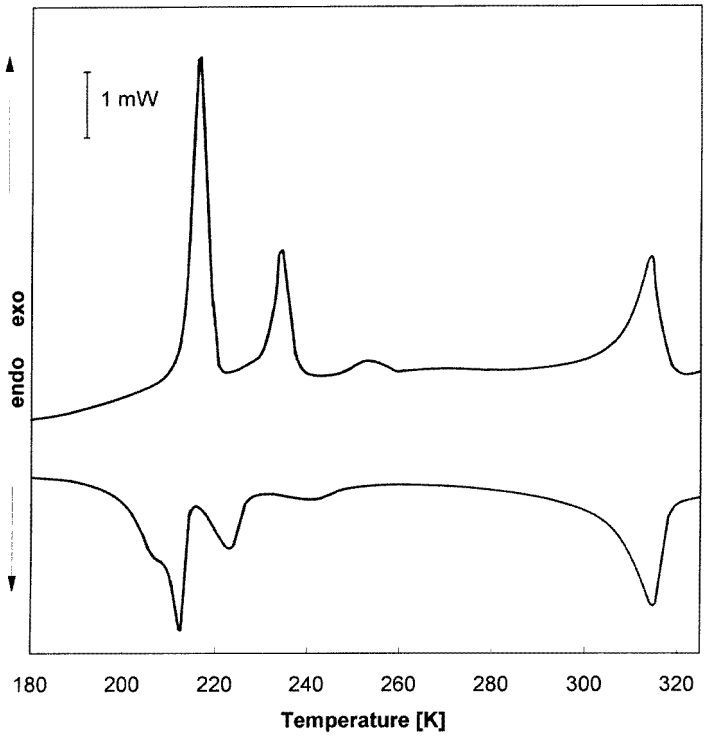

Figure 5. DCS curves of the metastable (β) form of the (n-$C_4H_9NH_3)_2BiCl_5$ crystal recorded on heating and cooling (sample mass, 20.1 mg; scanning rate, 10 K min^{-1}).

Table 5. The transition temperatures, enthalpies, entropies and character of the phase transition in the crystals of the n-butylammonium compounds (temperatures on heating).

Compound	T_c (K)	ΔH_{tr} (kJ mol^{-1})	ΔS_{tr} (J mol^{-1} K^{-1})	Order of phase transition
(n-$C_4H_9NH_3)_3SbCl_6$	322 ($\Delta T = 5$ K)	4.4	13.6	First
(n-$C_4H_9NH_3)_2SbCl_5$	315	0.36	1.1	Second
	229	1.79	7.5	Mixed (first and second)
(n-$C_4H_9NH_3)_2BiCl_5$, $\alpha \rightarrow \beta$ (phase transition)				
	$\simeq$ 370			Mixed (first and second) irreversible
β form	310	0.53	1.7	Second
	250 ($\Delta T = 6$ K)	0.05	0.2	Weak first
	232 ($\Delta T = 6$ K)	0.267	1.15	First
	215 ($\Delta T \simeq 2$ K)	1.18	5.5	First

to be of the displacive type rather than of the order–disorder type. However, the martensitic (diffusionless displacive first-order) type of the above-mentioned phase transitions in the title crystals may not be excluded but it would require further investigation by means of very accurate adiabatic calorimetric studies. The martensitic phase transitions have been rather rarely encountered up to now in ionic crystals (e.g. $(CH_3NH_3)_2[TeCl_6]$ [18] and $BaTiO_3$ [19]).

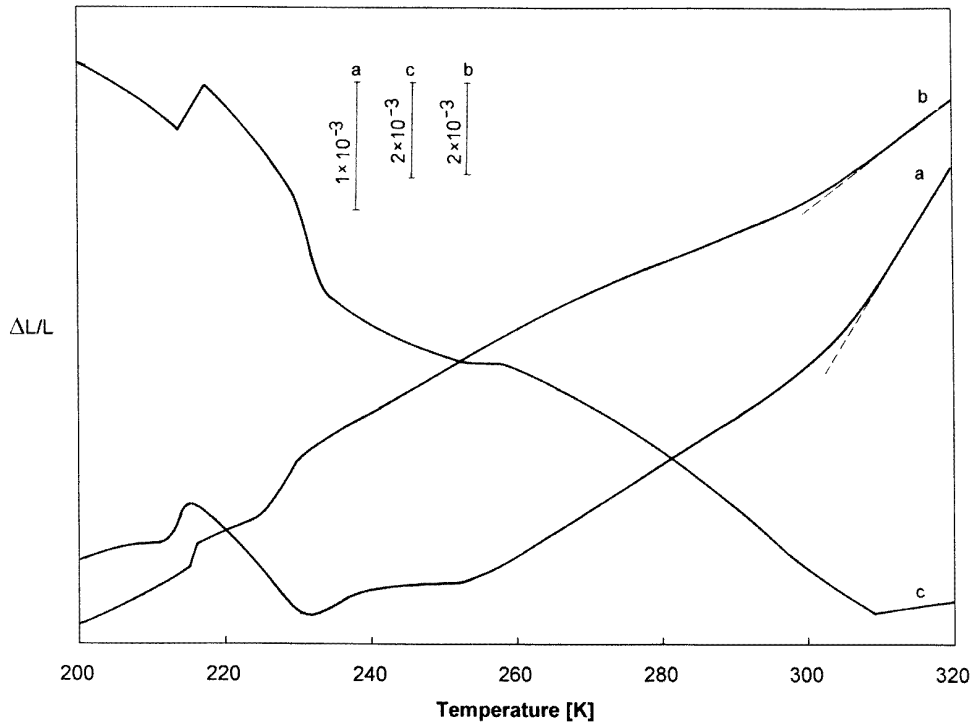

Figure 6. Temperature dependence of the linear thermal expansion $\Delta L/L$ measured along the a, b and c directions in the vicinity of the phase transitions at 215, 232, 250 and 310 K for the metastable (β) form of the (n-$C_4H_9NH_3)_2BiCl_5$ crystal.

3.3. Dilatometric measurements

The temperature dependences of the linear thermal expansion along the a, b and c axes between 320 and 190 K for (n-$C_4H_9NH_3)_2BiCl_5$ are shown in figure 6. Anomalous changes in dilation of this crystal observed in the vicinity of 310, 253, 230.5 and 214 K (recorded on heating) correspond to the phase transitions found by calorimetric measurements at 310, 250, 232 and 215 K, respectively. The continuous nature of the phase transition at 310 K has been confirmed. The discontinuous character and the thermal hysteresis observed ($\Delta T = 7$ and 3 K) confirmed the first-order character of the last two phase transitions. Similar values of thermal hysteresis for these phase transitions were found by DSC. The dilatometric data for the phase transition at 250 K suggest a continuous type of the phase transition in contrast with the first-order type from the DSC experiment. The pressure coefficient for the first-order phase transition at 215 K (the best-shaped thermal anomaly) was estimated from the Clausius–Clapeyron relation: $dT_c/dp = \Delta V/\Delta S$ (where $\Delta V = +1.7 \times 10^{-3}$ is the change in the molar volume and ΔS is the value of the transition entropy) and amounts to $+8.9 \times 10^{-2}$ K MPa^{-1}.

The dilatometric measurements on the same sample of (n-$C_4H_9NH_3)_2BiCl_5$ were repeated 24 h later (on cooling). It turned out that the crystal exhibited only remnant thermal anomalies below room temperature. This means that after crossing the 370 K phase transition the (n-$C_4H_9NH_3)_2BiCl_5$ crystal is preserved in a metastable β form. Investigation of the time-dependent recovering process from such a metastable (β) form to the stable (α) form will be performed in the near future.

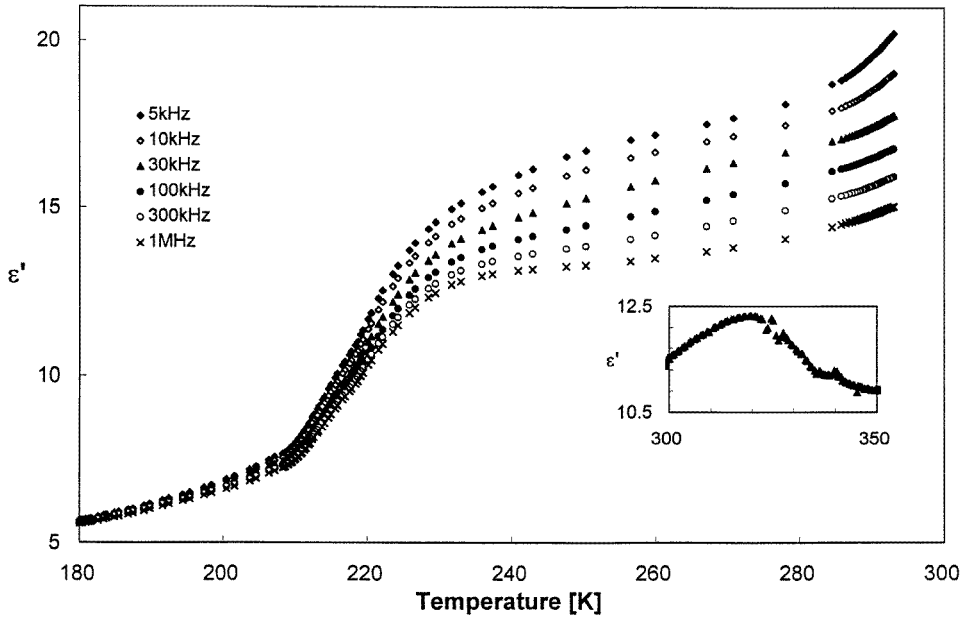

Figure 7. Temperature dependence of the real part of the complex electric permittivity for the polycrystalline sample of the $(n\text{-}C_4H_9NH_3)_2SbCl_5$ crystal between 5 kHz and 1 MHz in the vicinity of the phase transition at 229 K. The inset of figure shows the temperature dependence of ε' measured at 30 kHz for the single-crystal sample in the vicinity of the phase transition at 315 K.

3.4. Dielectric studies

The dielectric measurements of $(n\text{-}C_4H_9NH_3)_2SbCl_5$ were performed both for the polycrystalline and for the single-crystal samples (along only one direction). The temperature dependence of the real part ε' of the complex electric permittivity ε^* between 5 kHz and 1 MHz in the low-temperature region for the polycrystalline sample is shown in figure 7. The phase transition at 229 K is accompanied by a rapid decrease in ε' by several units. Above 229 K a distinct relaxation process should be noted. The strength of the relaxator decreases on approaching the phase transition. This low-frequency relaxation process probably overlaps the electric conductivity at room temperature. The higher-temperature phase transition at 315 K is visible only for the single-crystal samples which were prepared perpendicular to the cleavage plane (no crystal structure data are available so far). This phase transition is characterized by a broad maximum of ε' which is independent of frequency.

The results of the dielectric measurements obtained for the $(n\text{-}C_4H_9NH_3)_3SbCl_6$ crystal for the polycrystalline sample are presented in figure 8. The temperature dependence of ε' measured at 1 MHz, on cooling, above room temperature reveals one small broad anomaly in ε' at 317 K which confirms the phase transition found by DSC measurements. No relaxation process was found close to the phase transition region between 1 kHz and 1 MHz.

The $(n\text{-}C_4H_9NH_3)_2BiCl_5$ crystals appears to be very interesting from the dielectric point of view. The temperature dependence of the real part of the complex electric permittivity measured at 1 MHz along the c direction in the first heating process between 300 and 400 K is shown in figure 9 (lower curve). Starting from room temperature, the ε'_c-value

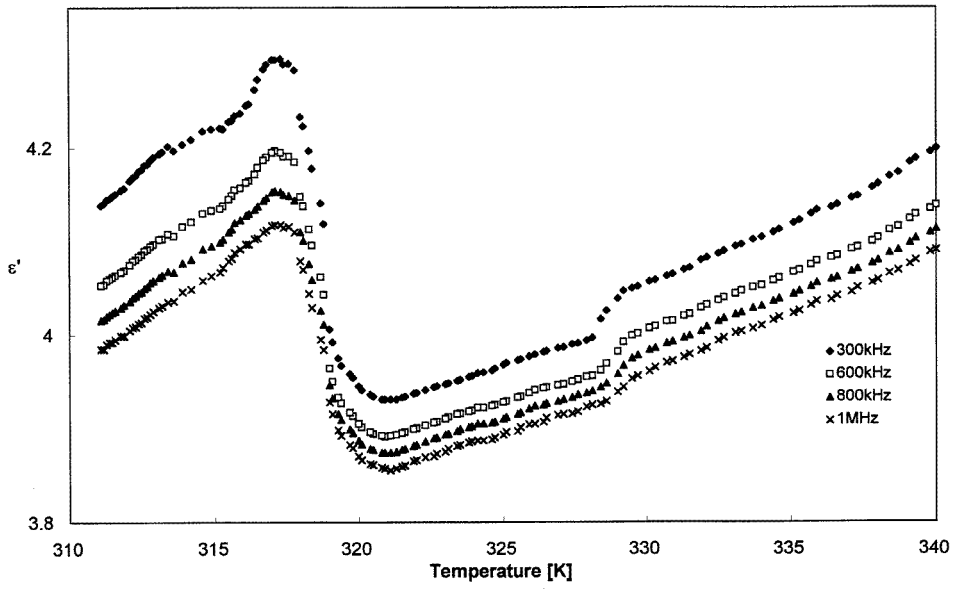

Figure 8. Temperature dependence of the real part ε' of the complex electric permittivity for the polycrystalline sample (on cooling) in the vicinity of the phase transition at 317 K for $(n\text{-}C_4H_9NH_3)_2SbCl_5$ between 300 kHz and 1 MHz.

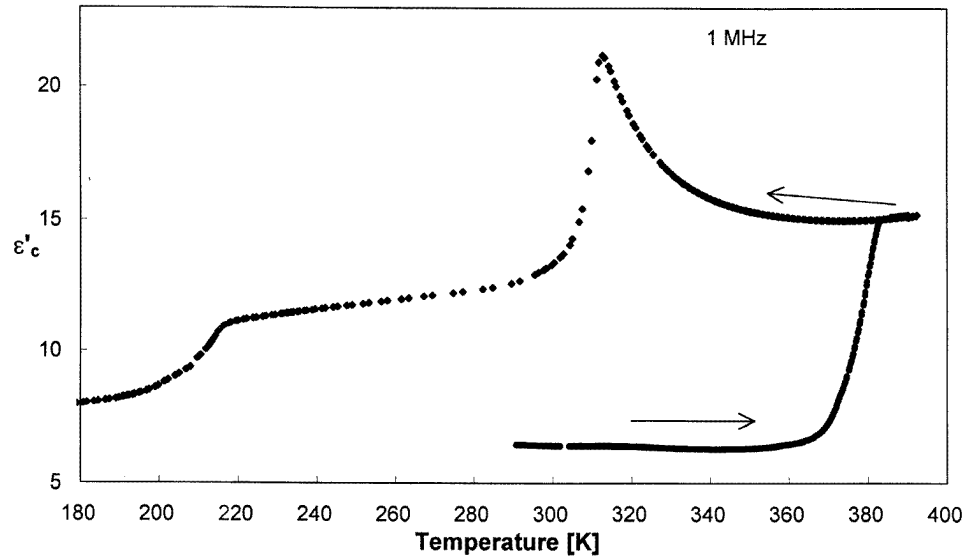

Figure 9. Temperature dependence of the real part of the complex electric permittivity for the $(n\text{-}C_4H_9NH_3)_2BiCl_5$ crystal along the c axis at 1 MHz.

changes slightly with increasing temperature and above 370 K it increases rapidly by about 8 units. This anomaly corresponds to the irreversible phase transition found by the DSC measurements. During the cooling process of the $(n\text{-}C_4H_9NH_3)_2BiCl_5$ crystal in the β

metastable form from 400 K the ε_c'-value continuously increases, exhibiting a distinct peak at 310 K which is characteristic of the second-order phase transition. The anomaly in the $\varepsilon_c'(T)$ curve displayed below 215 K is typical of discontinuous transitions. It is important to notice that the phase transitions at 232 and 250 K are inactive in the dielectric measurements. Within experimental accuracy the peak of ε_c' at about 310 K seems to occur at the same temperature, for all measured frequencies between 1 kHz and 1 MHz. No dielectric dispersion both above 310 K and close to 215 K in the low-frequency region was observed. It was found that the static dielectric permittivity ε_c at 1 MHz obeys the Curie–Weiss law around $T_c = 310$ K with the Curie constants $C_+ = 1155$ and $C_- = 267$. The ratio of these Curie constants ($C_+/C_- = 4.3$) is considerably larger than expected for the ordinary second-order ferroelectric phase transition.

The dielectric measurements for the β form of $(n\text{-}C_4H_9NH_3)_2BiCl_5$ carried out in the microwave frequency region, from 30 to 800 MHz, reveal a distinct relaxation process around the high-temperature phase transition at 310 K (figure 10). The maximum value of ε_c' decreases and the positions of the peaks shift towards higher temperatures as the frequency increases. These results indicate the occurrence of the 'critical slowing down' of the macroscopic relaxation time in the high-temperature phase (for $T > 310$ K) when the phase transition is approached. It is known that, for ferroelectric crystals of the second-order phase transition, a typical double peak for ε' usually appears close to T_c [21]. In this case, however, only a single-peak anomaly is observed in the measured frequency region. Figure 11 shows the Cole–Cole plots at several temperatures above $T_c = 310$ K. The experimental points are well described by the Cole–Cole arc law with the following formula:

$$\varepsilon^*(\omega) = \varepsilon_\infty + \frac{\varepsilon_0 - \varepsilon_\infty}{1 + (\mathrm{i}\omega\tau)^\beta}$$

where $\varepsilon^*(\omega) = \varepsilon' - \mathrm{i}\varepsilon''$, and ε_0 and ε_∞ are the electric permittivity at low- and high-frequency limits, respectively. τ is the macroscopic relaxation time and β measures the deviation from the Debye semicircle, representing the distribution of the relaxation times. The values of the β parameter estimated by least-squares fitting is greater than 0.95 in the temperature range 325–310 K. It indicates the monodispersive nature of the relaxation process above 310 K. In order to estimate the activation energy of the thermally activated process in non-ferroelectric crystals usually the $\ln\tau = f(1/T)$ expression is used provided that τ exhibits a weak temperature dependence. In this case, however, the macroscopic relaxation time exhibits a distinct temperature dependence approaching the phase transition point (which is equivalent to a critical increase in the $(\varepsilon_0 - \varepsilon_\infty)$ increment). The activation energy (70 kJ mol^{-1}) calculated for the $(n\text{-}C_4H_9NH_3)_2BiCl_5$ crystal, using the above formula, seems to be too high and rather non-realistic. This activation energy per 1 mol of the cations is therefore equal to about 35 kJ mol^{-1} assuming that two crystallographically independent *n*-butylammonium cations are distinguished in the crystal. This value corresponds to the energy sufficient for breaking off at least two strong NH...Cl hydrogen bonds. The spectroscopic studies (IR and Raman [22]) show, however, that in the metastable β form of $(n\text{-}C_4H_9NH_3)_2BiCl_5$ the *n*-butylammonium cations form weak NH...Cl hydrogen bonds; therefore the activation energy should be distinctly smaller.

According to the molecular-field approximation for crystals exhibiting an important change in $(\varepsilon_0 - \varepsilon_\infty)$ with temperature close to transition point the relationship between the macroscopic relaxation time τ and temperature T is given by the formula [23]

$$\tau = (h/k_B C)(\varepsilon_0 - \varepsilon_\infty)\exp(E_a/k_B T)$$

where E_a is the activation energy, C the Curie–Weiss constant, k_B the Boltzmann constant

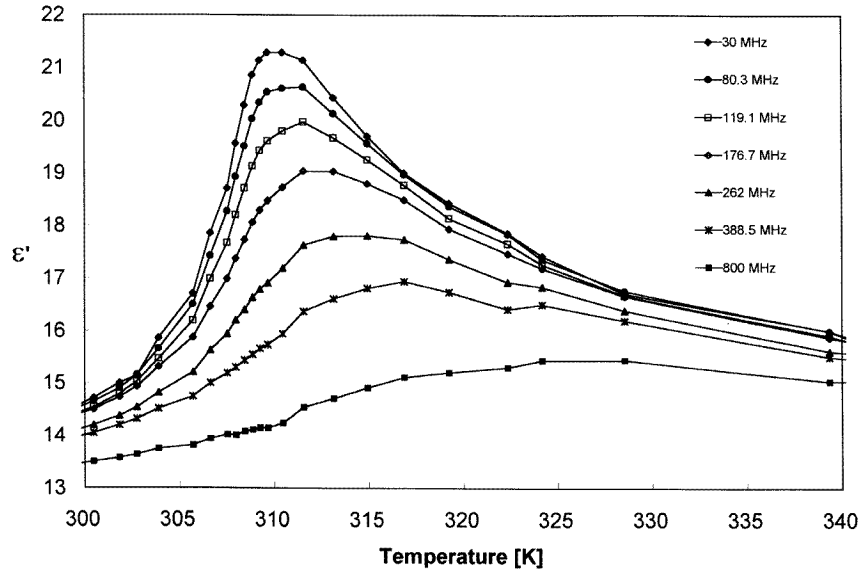

(a)

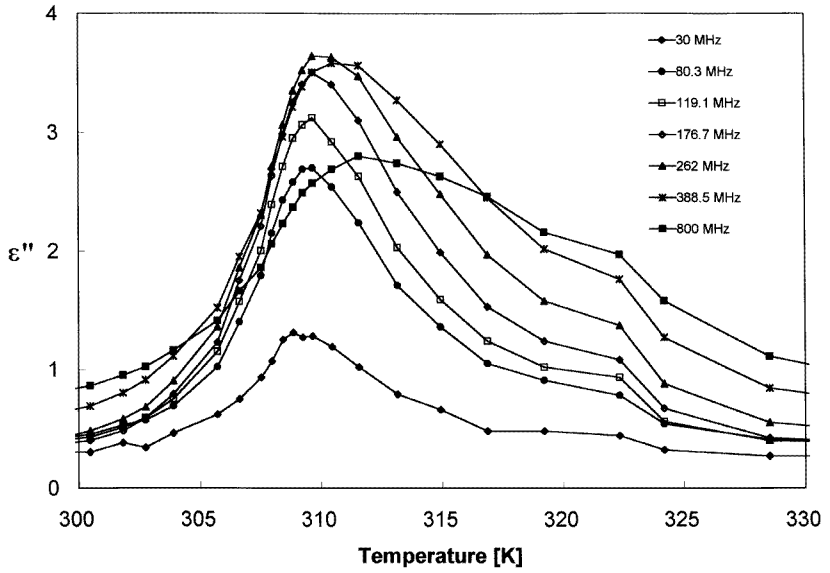

(b)

Figure 10. Temperature dependences of (a) the real and (b) the imaginary parts of the complex electric permittivity at frequencies from 30 to 800 MHz (on cooling) for the β form of the $(n\text{-}C_4H_9NH_3)_2BiCl_5$ crystal along the c axis around the phase transition at 310 K.

and h the Planck constant. The activation energy estimated in this way (figure 12) is equal to 16 kJ mol^{-1} and this value is more justified and consistent with the spectroscopic studies. In some alkylammonium crystals in which cations are bonded with the comparable strength

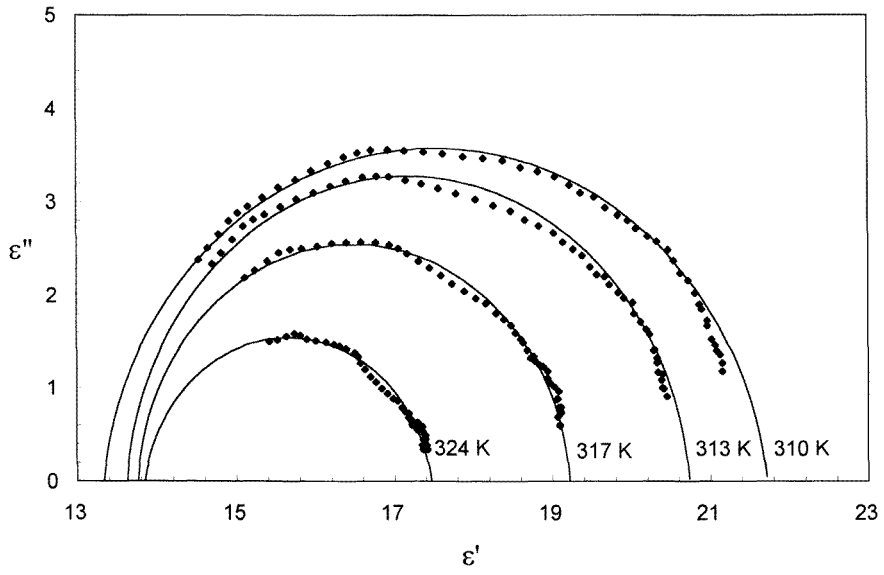

Figure 11. Cole–Cole diagrams of the electric permittivity measured along the c axis of (n-$C_4H_9NH_3)_2BiCl_5$ in the frequency range from 30 to 800 MHz.

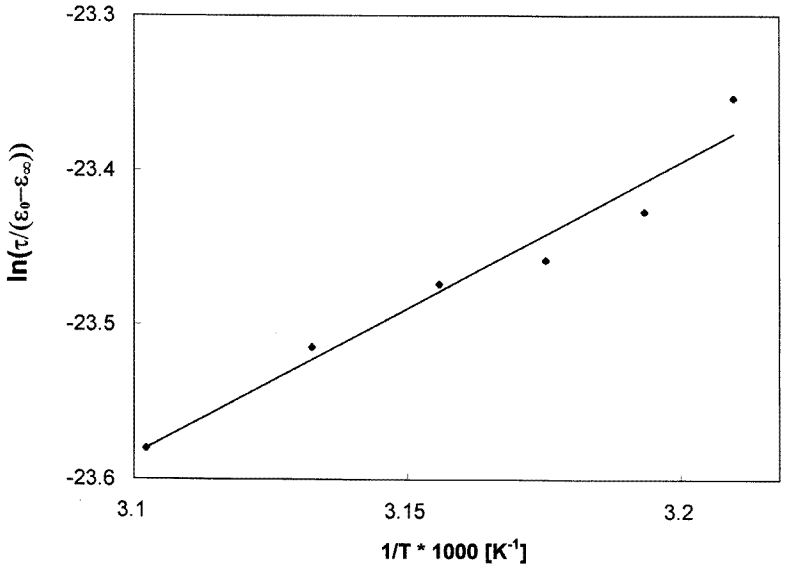

Figure 12. The relation between the $\ln \tau/(\varepsilon_0 - \varepsilon_\infty)$ and $1/T$ plot above 310 K of the β form of (n-$C_4H_9NH_3)_2BiCl_5$.

of the N–H . . . Cl hydrogen bonding a similar value of the activation energy was found from the dielectric dispersion studies [24, 25].

The dielectric response in the vicinity of the 310 K phase transition for the (n-$C_4H_9NH_3)_2BiCl_5$ crystal indicates that the dipole–dipole interactions become relatively

strong when approaching the critical point. Such behaviour may suggest the possibility of appearance of long-range order in this material. To verify this suggestion the pyroelectric effect was checked between 400 and 200 K using the pyroelectric charge method. Unfortunately, such measurements were performed only for two directions, namely along the c axis and for one of the crystallographic directions perpendicular to the c axis. (We did not succeed in obtaining a good-quality single crystal large enough to be able to prepare samples perpendicular to all crystallographic axes.) No pyroelectric current was observed in the temperature region between 310 and 200 K. We should add, however, that above 370 K the single crystal becomes strongly defected (cracked). This means that we are not able to use a DC electric field higher than 300 V cm^{-1}, which might be too small to obtain a single-domain state for the β form of $(n\text{-}C_4H_9NH_3)_2BiCl_5$.

4. Discussion

The phase transformations in all the crystals of the n-butylammonium compounds are due to thermal motions of the organic cations which cause changes in the hydrogen bonding between the ammonium cation and the chlorine ions as is observed in crystals of the shorter-chain compounds of the general formula $(C_nH_{2n+1}NH_3)_2MCl_4$ (M = Zn, Co, Cu or Mn) [26] and $(C_nH_{2n+1}NH_3)_3M_2X_9$ (M = Sb or Bi; X = Cl, Br or I) [1].

The crystals of the n-butylammonium compounds the chloroantimonates(III) presented in this paper, $[(n\text{-}C_4H_9NH_3)_3SbCl_6$ and $(n\text{-}C_4H_9NH_3)_2SbCl_5]$, differ from each other in both the number of phase transitions and the transition enthalpies. The differences between the dynamical properties of these two crystals may be attributed to various inorganic sublattices characteristic of these compounds, which influence the thermal motion of the cations. The $(n\text{-}C_4H_9NH_3)_3SbCl_6$ crystals possess an anionic sublattice built of isolated $SbCl_6^{3-}$ octahedra, while for the $(n\text{-}C_4H_9NH_3)_2SbCl_5$ crystal the sublattice consists of isolated $Sb_2Cl_{10}^{4-}$ units composed of two octahedra sharing an edge. It seems that the anionic sublattice influences the packing of cations and indirectly also their thermal motions.

The $(n\text{-}C_4H_9NH_3)_2SbCl_5$ and $(n\text{-}C_4H_9NH_3)_2BiCl_5$ crystals, which were expected to be isomorphous, also revealed different thermodynamic properties. In the former crystal, which most probably possesses large conformational disorder of the alkyl chains, the phase transformation occurs on heating at $T_c = 315$ K without breakdown of the lattice. The bismuth analogue $(n\text{-}C_4H_9NH_3)_2BiCl_5$ revealed only remnant disorder for one of the two non-equivalent organic cations at room temperature. The disorder is realized by splitting of the C(3) carbon atom of the alkyl chain between two sites with the occupancy factors 0.5. Assuming that the disorder is dynamical in nature, it would correspond to the rotation of the ethyl C(3)–C(4) group of the alkyl chain around the single C(1)–C(2) bond. Such a motion gives only a minor contribution to the dielectric permittivity. This motion is continuously slowed on cooling; however, it does not lead to the phase transition. This is confirmed by experiment since neither a dielectric nor a DSC anomaly is observed on cooling in the normal (α) form. During heating of the $(n\text{-}C_4H_9NH_3)_2BiCl_5$ crystals above room temperature, increasing disorder of the alkyl groups causes breakdown of the crystal lattice, before the melting point is reached. Essential distortion of the anionic sublattice appears. This causes weakening of the hydrogen bonding and leads to an increase in the freedom of the reorientational motion of the cations. This was recently confirmed by Raman studies around the $\alpha \rightarrow \beta$-phase transition [22].

The phase transition at 215 K for the β form of the $(n\text{-}C_4H_9NH_3)_2BiCl_5$ crystal is dielectrically active ($\Delta\varepsilon \approx 4$) whereas the phase transitions at 232 and 250 K are invisible. The suggestion based on the DSC measurements that the 215 K phase transition is of an order–disorder type ($\Delta S = 5.5$ J mol^{-1} K^{-1}) was recently confirmed by a Raman investigation [22]. It turns out that at 215 K the most spectacular changes in the spectra were found in the cation internal vibration region (e.g. $\delta^{sym}(NH_3^+)$ and $\delta^{as}(CH_3)$) which indicates the changes in the motional state of *n*-butylammonium cations.

On the other hand the induced dipole moment around the 232 and 250 K phase transitions is too small to detect by the dielectric methods. There are two possible explanations for this behaviour: firstly the reorientation is due to the rotation of the weakly polar methyl groups around their C_3 axis and secondly, which is more probable, the phase transition is involved with the deformation in inorganic sublattice (the displacive mechanism) with a very small induced dipole moment.

The dielectric response that was found in the metastable β form of the $(n\text{-}C_4H_9NH_3)_2BiCl_5$ crystal around 310 K resembles those found in the $(n\text{-}C_3H_7NH_3)_3Sb_2Cl_9$ crystal (containing shorter *n*-propylammonium cations) at the 232 K phase transition [13]. In both crystals the monodispersive character of relaxation process appears. The frequency ranges of observed dispersion are comparable for these two crystals, with a macroscopic relaxation time of the order of 10^{-9} s. In addition, which is more interesting, the dielectric increments are almost the same; $\varepsilon_0 - \varepsilon_\infty$ is of the order of 10 units. From the structural investigations of the *n*-propylammonium compound it is known that the dielectric absorption is related to the reorientation of the alkyl groups around the long axis of the cation. In the case of the n-butylammonium compound, in spite of the fact that the type of disorder is not precisely known in the metastable β form, the significant similarity of the dielectric parameters of the compared crystals suggests a similar molecular mechanism of the relaxation process. We should also emphasize that the dielectric response found in the microwave frequency region unequivocally indicates an order–disorder mechanism of the continuous phase transition at 310 K for $(n\text{-}C_4H_9NH_3)_2BiCl_5$ in spite of the small value of $\Delta S \approx 1.7$ J mol^{-1} K^{-1} accompanying this transition.

The $(n\text{-}C_4H_9NH_3)_2BiCl_5$ crystal undergoes a transition to a new metastable form (β), which is characterized by the important conformational disorder of the alkyl chains. As the result of this we could observe a complex sequence of phase transitions on cooling. The disruption of the lattice close to the 370 K transition is not permanent. After some time the crystal returns, however, to the stable α form. The nature of the transformation to the metastable β form is unclear. It may be argued that it is similar to the type of reorientations found in many crystals of the $(C_nH_{2n+1}NH_3)_2MCl_4$ (M = Zn, Co, Cu and Mn) family [26], namely the precession of the alkyl groups around the long axis of the molecule.

The molecular mechanism of the phase transitions found in the title crystals seems to be rather complex. Apart from the order–disorder phase transitions characterized by a relatively large entropy effect, phase transitions accompanied by small entropy changes were also found. The latter phase transitions probably have their origin in the deformation in the inorganic sublattice and this requires confirmation by other methods.

The investigations of the polar properties lead to the conclusion that the polar properties (ferroelectric and pyroelectric) are not observed in halogenoantimonates(III) and halogenobismuthates(III) crystals containing bulky cations. Nevertheless the presence of the long linear alkyl groups in the lattice (*n*-propylammonium and *n*-butylammonium groups) favours the dipole–dipole interactions which leads to distinct dielectric anomalies at the phase transitions. On the other hand the dipole–dipole interactions are very weak in

the crystals containing tertiary (branched) cations, e.g. the crystals of isopropylammonium compounds [9].

5. Conclusion

(1) The phase transitions found in n-butylammonium derivatives $(n\text{-}C_4H_9NH_3)_2SbCl_5$ (322 K), $(n\text{-}C_4H_9NH_3)_2BiCl_5$ (310 and 215 K) and $(n\text{-}C_4H_9NH_3)_3SbCl_6$ (229 K) exhibit an 'order–disorder' character.

(2) The microscopic origin of the order–disorder phase transitions should be related to the freezing of the dynamical disorder of the NH...Cl hydrogen bonding and to the corresponding tilting of hydrocarbon chains.

(3) The 370 K phase transition in $(n\text{-}C_4H_9NH_3)_2BiCl_5$ is postulated to exist between the stable (α) and the metastable (β) form.

(4) A distinct relaxation process exhibiting the 'critical slowing down' features around the 310 K phase transition is found in the β form (metastable) of the $(C_4H_9NH_3)_2BiCl_5$ crystal.

Acknowledgment

This work was supported by KBN project 3 T09A 093 10.

References

[1] Jakubas R and Sobczyk L 1990 *Phase Trans.* **20** 163
[2] Varna V, Bhattarcharjee R, Vasan H N and Rao C N R 1992 *Spectrochim. Acta* A **48** 1631
[3] Ishihara H, Watanabe K, Iwata A, Yamada K, Kinoshita Y, Okuda T, Krishnan V G, Dou S and Weiss A 1992 *Z. Naturf.* a **47** 65
[4] Jakubas R, Krzewska U, Bator G and Sobczyk L 1988 *Ferroelectrics* **77** 129
[5] Jakubas R 1986 *Solid State Commun.* **60** 389
[6] Jakubas R, Miniewicz A, Bertault M, Sworakowski J and Collet A 1989 *J. Physique* **50** 1483
[7] Jakubas R 1989 *Solid State Commun.* **69** 267
[8] Jakubas R, Sobczyk L and Lefebvre J 1989 *Ferroelectrics* **100** 143
[9] Jakubas R, Bator G, Ciąpała P, Zaleski J, Baran J and Lefebvre J 1995 *J. Phys.: Condens. Matter* **7** 5335
[10] Jakubas R, Bator G, Foulon M, Lefebvre J and Matuszewski J 1993 *Z. Naturf.* a **48** 529
[11] Okuda T, Tanaka N, Ichiba S and Yamada K 1986 *Z. Naturf.* a **41** 319
[12] Jakubas R, Ciąpała P, Bator G, Ciunik Z, Decressain R, Lefebvre J and Baran J 1996 *Physica* B **217** 67
[13] Ciąpała P, Zaleski J, Bator G, Jakubas R and Pietraszko A 1996 *J. Phys.: Condens. Matter* **8** 1957
[14] *SHELXTL PC Program System* 1990 (Madison, Wisconsin: Siemens Analytical X-ray Instruments)
[15] Zaleski J and Pietraszko A 1996 *Acta Crystallogr.* B **52** 287
[16] Prassides K, Day P and Cheetham A K 1985 *Inorg. Chem.* **24** 545
[17] Bigolli F, Lanfranchi M and Pellinghelli M A 1984 *Inorg. Chim. Acta* **90** 215
[18] Onoda N, Matsuo T and Suga H 1988 *Phil. Mag.* **57** 245
[19] Kimura T, Newnham R E and Cross E 1981 *Phase Trans.* **2** 113
[20] Devonshire A F 1949 *Phil. Mag.* **40** 1040
[21] Yoshimitsu K and Matsubara T 1968 *Prog. Theor Phys.* Suppl. 109
[22] Bator G, Provoost R, Silverans R E and Zeegers-Huyskens Th 1996 *J. Mol. Struct.* submitted
[23] Makita Y and Seo I 1969 *J. Chem. Phys.* **51** 3058
[24] Jakubas R, Narewski E and Sobczyk L 1986 *Phys. Status Solidi* a **98** K 115
[25] Bator G and Jakubas R 1995 *Phys. Status Solidi* a **147** 591
[26] Arend H, Huber W, Mischgowsky F H and Richter-van Leeven G K 1978 *J. Cryst. Growth* **43** 213